Modulated Phase-Shifting for 3D Scanning

Tongbo Chen Hans-Peter Seidel Hendrik P. A. Lensch
MPI Informatik

Abstract

We present a new 3D scanning method using modulated phase-shifting. Optical scanning of complex objects or scenes with significant global light transport, such as subsurface scattering, interreflections, volumetric scattering, etc. is a difficult task since the direct surface reflection will be mixed with the global illumination. The direct and global components can be efficiently separated using high frequency illumination which to some extend is done in traditional phase-shifting for 3D scanning. In this paper we introduce the concept of modulation based separation where a high frequency signal is multiplied on top of other signal. The modulated signal inherits the good separation properties of the high frequency signal and allows for removing artifacts due to global illumination. This technique can be used to clean up arbitrary projected signals, e.g. photographs as well as the sinusoid patterns used for phase-shifting. For the modulated phase-shifting, we propose a two-pass separation method exploiting high frequency patterns in two-dimensions that can filter out the global components much more completely than traditional one-pass separation methods. We demonstrate the effectiveness of our approach on a couple of scenes with significant subsurface scattering and interreflections.

1. Introduction

In structured light based 3D scanning, the 3D information is obtained by triangulation after establishing the correspondence between the camera pixels and the sub-pixel locations of the illuminating projector pixels. In order to establish this correspondence a large variety of patterns have been proposed [11], encoding the projector pixel locations. The decoding algorithms then assume that the measured camera pixels only locally depend on the projected patterns. This assumption is violated if global illumination effects such as interreflections or subsurface scattering are strong, leading to the observations of multiple overlaid signals. Most often these global illumination effects dampen high frequencies in the input patterns.

By choosing appropriate high frequency patterns, Nayar *et al*. [10] have demonstrated how global illumination effects can be separated from the direct illumination. Chen *et al*. [3] exploited this method for 3D scanning by using phase-shifting where the use of high-frequency sinusoid patterns drastically reduced the influence of the global illumination. The employed one-dimensional patterns (sinusoidal in x but constant in y), however, does not fully remove the global effects. It gets even worse for the lower frequency patterns that are required in temporal phase-unwrapping [7]. For these reasons, their method was combined with polarization difference imaging (PDI), exploiting the fact that multiply scattered light becomes depolarized. PDI on the other hand adds to the complexity of the setup and the acquisition. Furthermore, the combined effect of polarized illumination and the polarization characteristics of reflections at surfaces leads to a drastically weakened signal, especially at grazing angles [1].

In this paper we introduce modulation based separation, where the direct illumination component even of a low-frequency projected signal is correctly estimated. On top of the low-frequency signal we multiply a two-dimensional high frequency signal. We analyze the separation performance using high-frequency patterns in 1D or 2D, demonstrating that 2D separation patterns result in a much clearer separation. We further show that due to the non-linearity in the separation analysis, a sequential analysis of a 2D pattern once horizontally and once vertically produces an even better separation. Moreover, the modulation and separation scheme can be exploited for general low frequency patterns, such as an ordinary photograph.

The improved separation based on modulation with sequential analysis leads to a much better performance of 3D scanning. The proposed algorithm is more efficient with regard to subsurface scattering as well as interreflections than previous methods.

2. Related Work

In this section, we briefly review the recent advances in reflection component separation and their applications to 3D scanning of complex objects with global illumination effects. We also review the traditional phase-shifting methods for 3D scanning.

978-1-4244-2243-2/08/$25.00 ©2008 IEEE

2.1. Direct/Global Components Separation

The direct reflection component is due to a single reflection at the surface and is therefore directly correlated to the surface geometry. The global component is caused by multiple scattering events, such as interreflection or subsurface scattering. The global components can seriously deteriorate the measurements in 3D scanning [6]. Accurate 3D scanning methods for scenes with complex global light transport usually have a key component of removing or suppressing the global components. In [12], Seitz *et al*. presented a method for computing and removing interreflection in photographs of real scenes. Their method is based on Lambertian assumption and requires a very large number of images. Chen *et al*. [2] proposed an interactive photometric method to separate the specular reflection, one kind of direct component and to do 3D reconstruction from the estimated normal map. Their method can successfully deal with a class of translucent objects. Ma *et al*. [8] presented a rapid acquisition method of specular and diffuse normal maps from polarized spherical gradient illumination. Their method can produce high resolution 3D scans for moderately translucent objects, such as human faces. Based on the insight that direct and indirect scatter traces have different characteristics, Morris and Kutulakos [9] introduced a new 3D photography method, called scatter-trace photography. Their method provides new possibilities for 3D scanning of inhomogeneous transparent scenes. In [10] Nayar *et al*. introduced an efficient method for separating direct and global components by using high frequency illumination. Their approach is based on the insight that global light transport significantly dampens high frequencies in the incident illumination patterns while the direct reflections does not. In the same paper, they proposed several useful high frequency patterns, such as checkerboard patterns, sine patterns, *etc*. They also pointed out that phase-shifting can be used for 3D scanning. In [14], Talvala *et al*. adapted Nayar *et al*.'s separation method to remove veiling glare in high dynamic range imaging. They use a high frequency mask to selectively block the light that contributes to the veiling glare. Veeraraghavan *et al*. [15] presented a novel modulation-based method for capturing light field by using an attenuating mask. Chen *et al*. [3] extended Nayar *et al*.'s idea to 3D scanning of translucent objects. Their method is further enhanced by using parallel/cross polarization. In this paper, we also make use of Nayar *et al*.'s separation and propose a modulation technique where even for a low frequency input signal the direct component can be reliably estimated.

2.2. Phase-Shifting

Phase-shifting [13, 17] based on sinusoid patterns has been used extensively in optical 3D scanning. The source, usually a digital projector, projects a series of phase-shifted sinusoid patterns into the scene and a camera records the resulting image. From a sequence of shifted patterns one can detect for every camera pixel the phase within one period of the illuminating sinusoid pattern. The collective phase information is called the modulo 2π phase map. In order to determine the absolute position within the illumination pattern the period has to be localized. This process is called phase-unwrapping, for which lower frequency sinusoid patterns are typically used [5]. An unwrapped phase map directly encodes the correspondence between the image field and the projection field. Once this correspondence is determined, the 3D coordinate information of the object can be computed by triangulation.

Most of the advanced phased-shifting methods focus on the different aspects of the above procedure. With the increasingly ubiquitous availability of digital projectors and digital cameras, a typical setup of a phase-shifting system is a projector-camera system. However, the inaccuracy inherent in the commercial projectors introduces new problems. Zhang and Yau [19] proposed a new look-up-table method for phase error compensation. Instead of trying to improve scanning accuracy, some researchers are continuously working on the scanning speed. Zhang and Yau [20] presented a high-resolution, real-time phase-shifting method with customized hardware. Weise *et al*. [16] developed a fast 3D scanning system combining stereo and phase-shifting. Most of the high quality or high speed phase-shifting methods require an efficient phase-unwrapping method [5]. Zhang *et al*. [18] presented a multi-level quality guided phase-unwrapping for a real-time phase-shifting system. Huntley and Saldner [7] introduced the temporal phase-unwrapping method, which is a multi-scale method and very robust, especially when scanning highly discontinuous surfaces.

3. N-Step Phase-Shifting

In the past years, many different phase-shifting algorithms have been developed [5, 13, 17, 19, 20, 16, 18]. The measurement accuracy of phase-shifting is usually affected by the noise and inaccuracy of the source and sensor, *e.g*. imaging noise of the camera, and nonlinearity and light leakage of the projector. One of the most accurate methods is based on the N-step least squares phase-shifting algorithm [19] for a projector-camera system. Sinusoid patterns are generated by the projector and shifted by a factor of $\frac{2\pi}{N}$ for N times as

$$L_i(x, y) = 0.5 + 0.5\cos(2\pi fx + \delta_i), \qquad (1)$$

where (x, y) is the projector coordinate. The sinusoid is varying only in the x dimension. The frequency is denoted by f. $\delta_i = \frac{2\pi i}{N}, i = 1, 2, ..., N$ denote the N different phase shifts.

The camera records one image for each phase-shift and N images in total. The resulting intensity at camera pixel (x, y) in step i can be expressed as follows:

$$\begin{aligned} I_i(x,y) &= I^{'} + I^{''} cos(\Phi(x,y) + \delta_i) \\ &= a_0(x,y) + a_1(x,y)cos(\delta_i) + a_2(x,y)sin(\delta_i), \end{aligned} \quad (2)$$

where $I^{'}$ is the average intensity, $I^{''}$ the intensity amplitude, and Φ the phase to be solved. Solving the set of equations given in Eq. 2 in a least-square sense, we obtain,

$$\Phi(x,y) = tan^{-1}(\frac{-a_2(x,y)}{a_1(x,y)}), \quad (3)$$

where

$$[a_0(x,y)\ \ a_1(x,y)\ \ a_2(x,y)]^T = A^{-1}(\delta_i)B(x,y,\delta_i), \quad (4)$$

$$A(\delta_i) = \begin{bmatrix} N & \sum cos(\delta_i) & \sum sin(\delta_i) \\ \sum cos(\delta_i) & \sum cos^2(\delta_i) & \sum cos(\delta_i)sin(\delta_i) \\ \sum sin(\delta_i) & \sum cos(\delta_i)sin(\delta_i) & \sum sin^2(\delta_i) \end{bmatrix}, \quad (5)$$

and

$$B(x,y,\delta_i) = \Big[\sum I_i \ \ \sum I_i cos(\delta_i) \ \ \sum I_i sin(\delta_i)\Big]^T. \quad (6)$$

Using phase-shifting for 3D scanning, one is mostly interested in determining the effective phase $\Phi(x, y)$ which is correlated to the disparity and therefore the depth of the pixel. Additional phase-unwrapping employing lower frequency patterns is necessary to locate the period for which the phase is measured.

3.1. Separation Property

Following the idea presented in [10] one can exploit the different dependency of the direct and global illumination effects on a high frequency illumination pattern to separate these two components. Only the direct component L_d is correlated to the amplitude term $I^{''}$ while the global component L_g is not if and only if f is sufficiently high. Both L_d and L_g contribute to the average image $I^{'}$, or a_0. We compute L_d and L_g in the same way as in [3]:

$$\begin{aligned} L_d &= 2\sqrt{a_1^2 + a_2^2}, \quad \text{and} \\ L_g &= 2a_0 - 2\sqrt{a_1^2 + a_2^2}. \end{aligned} \quad (7)$$

Since there are 3 unknowns, a_0, a_1, and a_2, theoretically, 3 shifts are the minimum requirement for calculating the phase and the separation. In our experiments we apply either 6 or 8 shifts in order to alleviate distortions due to imaging noise, nonlinearity, vibration, *etc*.

In [10], Nayar *et al*. pointed out that the best separation of direct and global components is achieved with the highest frequency illumination patterns. In other words, the performance of the separation is limited by the frequency of the illumination. This highest frequency is however given by the properties of the projector and might be reduced due to light leakage and built-in image processing. In practice we apply $f = \frac{1}{6}$ as the overall highest frequency, and found $f = \frac{1}{8}$ with $N = 8$ to produce the best phase estimates. The unit for frequency is $cycles/pixel$. While there are practical limits to the highest reliable frequency the phase-shifting pattern furthermore is only of high frequency in the phase direction, here the x direction. It does not contain any high frequencies in the y direction and therefore has only limited descattering performance.

4. Modulated Phase-Shifting

In this section, we will introduce the modulated phase-shifting to improve the separation performance of traditional phase-shifting. The main idea is to modulate a high frequency signal, that has good separation performance on top of the low-frequency signal we might be interested in.

4.1. Modulation

In telecommunication, modulation is the process of varying a periodic waveform in order to carry another signal. Normally, a high-frequency sinusoid waveform is used as carrier signal. We perform modulation by multiplying an input signal L (sine waves for phase-shifting, see Eq. 1) with other shifted high frequency patterns. The process can be formally expressed as

$$\tilde{L}_{ij}(x,y) = L(x,y)M_x^i(x,y)M_y^j(x,y), \quad (8)$$

where $\tilde{L}$ is the modulated function to be projected. M_x is the modulation function in x dimension with frequency f_x and N_x shifts. Accordingly, M_y is a modulation function in the y dimension with frequency f_y and N_y shifts. The total number of projected images is N_xN_y. The highest frequency of the modulated signal is now given by either f_x or f_y and is no longer limited by the original signal's frequency since a multiplication in the spatial domain corresponds to a convolution in the frequency domain. Thus the modulated function $\tilde{L}$ has higher frequency than the non-modulated function L in both dimensions, and we can overall obtain a better separation of the direct/global components.

In principal, all the high frequency functions proposed in [10] for the separation can be used as modulation functions, M_x and M_y. We use either periodic binary functions or sinusoid functions as the modulation functions in all our experiments. The sinusoid modulation function is defined in the same way as L (see Eq. 1). The periodic binary function in x dimension is defined as

$$\mathcal{B}_x(x,y) = \lfloor 2xf \rfloor \bmod 2. \quad (9)$$

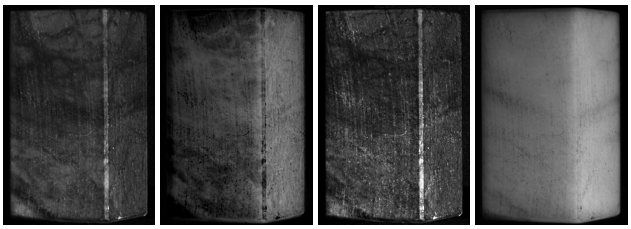

(a) (b) (c) (d)

Figure 1. Two-pass separation vs. one-pass 2D separation. Direct component (a) and global component (b) from the one-pass algorithm. Direct component (c) and global component (d) from the two-pass separation. Note that the two-pass separation method working on exactly the same input data produces a much clearer separation.

4.2. Multi-Pass Separation

In principle, a modulation in one direction is sufficient to perform some (possibly limited) separation. In this case, the separation into the direct and global components can be done using sinusoid functions and the analysis given in Eq. 7. One can also use a binary pattern. The separation is then computed as follows:

$$\begin{aligned} L_d(x,y) &= I_{max}(x,y) - I_{min}(x,y), \quad \text{and} \\ L_g(x.y) &= I_{min}(x,y). \end{aligned} \tag{10}$$

where $I_{max}(x,y)$ and $I_{min}(x,y)$ are the maximum and minimum intensities of pixel (x,y) for the N_x images.

In order to increase the separation performance one should perform the modulation in both dimensions to remove global illumination in both directions. Applying the modulation in 2D, one can simply apply the minimum-maximum approach on the $N_x N_y$ images and then evaluate Eq. 10, as that has been proposed by Nayar et al. [10].

It turns out, however, that a much better separation can be achieved by using sequential separation in each dimension. One can see the N_y images for a fixed step i in x as the 1D modulation of the "original" signal M_x^i with the modulation pattern M_y. Performing the 1D separation for every individual step in x then results in N_x direct component images L_d^i which act as the input to the second separation phase, this time in x. Note that we have used exactly the same input images as before but have a two-stage filtering where global illumination effects that might pass the first separation are filtered out in the second pass. The improved performance of the two-pass separation vs. the one-pass 2D minimum-maximum separation is demonstrated in Fig. 1.

4.3. Modulation for a General Signal

The idea of modulation based separation can be applied to more general signals. We demonstrate this by projecting an ordinary photograph into a scene inducing interreflections. In Fig. 2, the projected image is reflected off a glossy

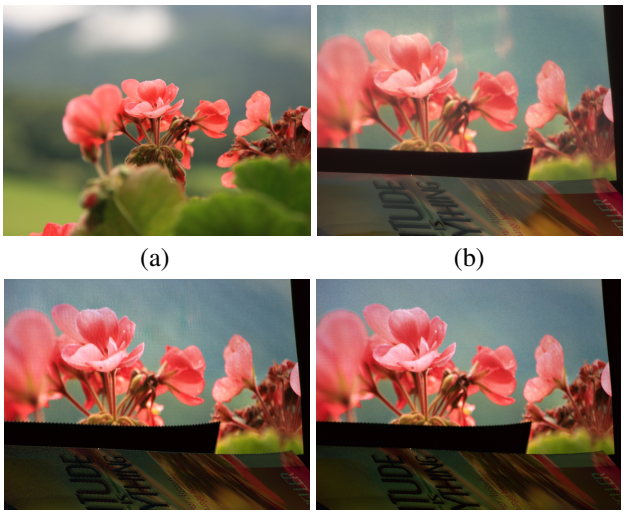

(a) (b) (c) (d)

Figure 2. An ordinary photograph (a) is projected into a scene containing a glossy surface at the bottom and a diffuse paper screen in the back. (b) The projected image in the back is polluted by the ghost image caused by the reflection from the glossy book cover. (c) The direct component separated by using 1D phase-shifting, with $f_x = \frac{1}{8}$ still contains some artifacts. (d) The two-pass separation algorithm, with $f = \frac{1}{8}$ in both dimensions suppresses the ghost image completely.

book cover causing a ghost image on the white paper screen in the back. The interreflection further reduces the contrast of the projected image. Moreover, the white paper is moderately translucent and induces subsurface scattering which reduces the sharpness of the projection. All these global illumination effects, interreflection and subsurface scattering cause the degeneration of the projection (see Fig. 2(b)). In order to suppress these artifacts, we first modulate the image using a sinusoid function with $f_x = \frac{1}{8}$ in x direction. This 1D separation (Fig. 2(c)) reduces the global illumination effects, but one can still notice some remaining artifacts. The image in Fig. 2(d) is obtained by using two-pass separation with a sinusoid of $f_x = \frac{1}{8}$ and a binary pattern with $f_y = \frac{1}{8}$. The additional second pass removes the ghost image completely and improves the contrast.

This example demonstrates the effectiveness of modulation and multi-pass separation in removing interreflection and subsurface scattering effects even for general input signals. More generally, any low frequency input signal could be modulated to inherit the separation properties of the high frequency modulation function.

4.4. Modulated Phase-Shifting and Unwrapping

In the case of phase-shifting, the original patterns L are already one-dimensional sinusoids that inherently perform 1D separation for sufficiently high frequencies f_x. For temporal phase-unwrapping [7, 3] a series of different frequen-

cies is applied, *e.g.* $\frac{1}{1024}$, $\frac{1}{512}$, $\frac{1}{256}$, $\frac{1}{128}$, $\frac{1}{64}$, $\frac{1}{32}$, $\frac{1}{16}$, and $\frac{1}{8}$. The highest frequencies are used for estimating the phase while the lower frequencies are required to unwrap the phase.

In order to obtain measurements that are robust to global illumination effects we apply a modulation in the y direction using a shifted high frequency pattern on top of the original phase-shifting signal and then perform the two-pass separation presented in the previous sections. The first pass, operating in the y direction, only performs the direct/global separation. The second pass is then used for both filtering out the global component that might have survived the first pass and for determining the phase or performing the unwrapping.

In theory, for the low frequencies a modulation in x and y would be necessary to remove any influence of global illumination effects on the unwrapping. In practice, since the low frequencies are only used to determine the period and not the phase, the unwrapping turns out to be stable enough even without any modulation in all our test cases.

Modulation is therefore only applied to the high frequency signals used to estimate the phase with $f_x = \frac{1}{8}$ or $f_x = \frac{1}{16}$. Since the frequencies in x are high enough to obtain reasonable separation performance, a modulation in y is sufficient. For the 3D scans presented in this paper we applied a modulation frequency of $f_y = \frac{1}{6}$ with 6 shifts, leading to six times the number of images for the highest frequency. However, since no modulation is required for the lower frequencies the overhead for the whole 3D scanning using modulated phase-shifting is quite moderate.

5. Results

In this section we describe the experimental setup and demonstrate the effectiveness of our method in removing subsurface scattering and interreflections during 3D scanning. We show results for both planar (a face of an alabaster block) or non-planar objects (an edge of an alabaster block and an alabaster horse head). We also show results for a scene including high frequency interreflection (a glossy sphere in a corner). The four scenes are presented in Fig. 3.

Our basic acquisition system consists of only one projector and one camera capturing images. In the current setup, we use a Mitsubishi XD490U XGA DLP projector (with 1024×768 pixels) and a 14-bit 1360×1024-pixel ProgRes®C14*plus* CCD camera. For comparison with polarization difference imaging enhanced phase-shifting [3], we use two additional linear polarizers, one for the camera and the other for the projector. The camera's response curve is recovered using the method proposed by Debevec and Malik [4] and HDR images are taken by fusing multiple images with different exposure times. We calibrate the projector-camera system geometrically using Zhang's method [21].

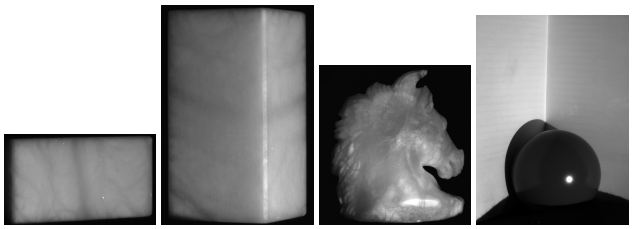

(a) (b) (c) (d)

Figure 3. Photographs of the experimental scenes. (a) One face of an alabaster block. (b) One edge of an alabaster block. (c) An alabaster horse head. (d) A glossy sphere in the corner of an open notebook.

5.1. Alabaster Plane

In the first example we perform 3D scanning on a planar slab of highly translucent alabaster with significant subsurface structures (Fig. 4). Performing phase-shifting with 1D patterns of frequency $f_x = \frac{1}{8}$ separates out some of the subsurface scattering but gets corrupted by structures close to the surface. Applying polarization difference imaging filters out the depolarized multiply scattered components but also weakens the signal, resulting in a less biased but slightly noisier reconstructed geometry. An even better separation with a higher frequency signal is obtained by modulating the phase-shifting signal by a second sinusoid in the y direction of frequency $f = \frac{1}{6}$, following the approach outlined in the previous sections. The separated direct component and the resulting 3D geometry is almost free of subsurface structures and slightly smoother than the reconstruction based on PDI.

This increase in quality comes at a small cost in the time required for acquisition: For 1D phase-shifting, we applied 8 different shifts. For PDI this 8-image sequence is actually captured twice (16 images in total) for two different orientations of the camera polarization filter. In the modulated phase-shifting we added three phase shifts in the y direction amounting to $3 \times 8 = 24$ images.

The benefit of modulating a traditional phase-shifting pattern gets even more apparent if the original signal has lower frequency. In Fig. 5, the dark veins of the alabaster cause some clear marks in the reconstructed geometry when applying traditional 1D phase-shifting with $f_x = \frac{1}{16}$. Modulating with a binary pattern of frequency $f_y = \frac{1}{6}$ again brings out a much better separated direct component and an unbiased 3D shape. The effectiveness of modulated phase-shifting (MPS) to obtain accurate results even for low frequencies is of high importance for phase-shifting with temporal phase unwrapping where it brings two benefits: Phase-maps generated with lower frequencies typically carry slightly less noise than those obtained from higher frequencies. Furthermore, they are easier to unwrap because there are less ambiguous periods.

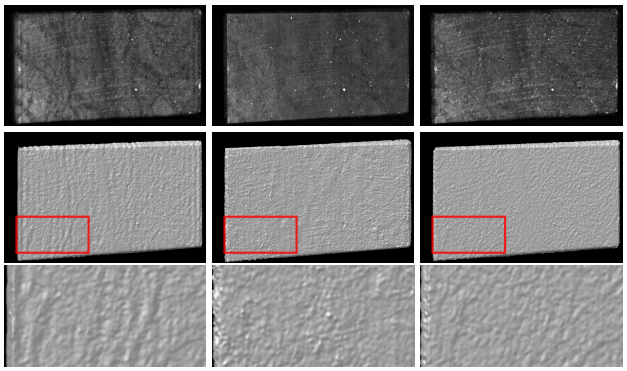

(a) (b) (c)

Figure 4. Separated direct components (first row) and reconstructed 3D shapes (second row) for the alabaster slab. (a) Standard phase-shifting (PS) with $f_x = \frac{1}{8}$. (b) Polarization difference imaging (PDI) with $f_x = \frac{1}{8}$. (c) Modulated phase-shifting (MPS) with $f_x = \frac{1}{8}$ and $f_y = \frac{1}{6}$. The subsurface structures that are corrupting the 3D reconstruction in (a) have been successfully filtered out by both PDI and MPS.

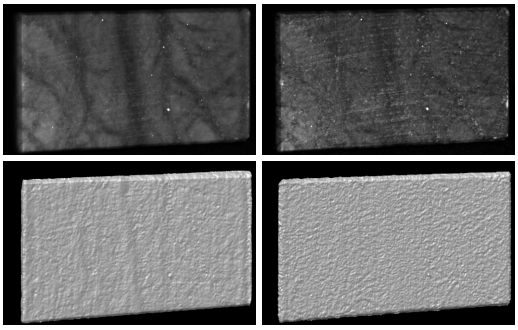

(a) (b)

Figure 5. Direct components and 3D shapes for the alabaster block with lower frequencies. (a) PS with $f_x = \frac{1}{16}$. (b) MPS with $f_x = \frac{1}{16}$ and $f_y = \frac{1}{6}$. The subsurface structures influence the estimated geometry from PS.

5.2. Alabaster Edge

While in the previous example PDI and our MPS have demonstrated rather similar performance we obtained rather different results on the second experiment where we rotated the alabaster block to capture one of its edges (Fig. 6). Due to the different orientation of the normals which influence the polarization even of the direct reflection the measured direct component in the PDI is much darker. The noise in the 3D reconstruction by PDI is clearly noticeable. Standard phase-shifting still contains too much subsurface scattering which can be removed effectively using modulation.

5.3. Alabaster Horse Head

A slightly better performance of the PDI approach is visible in the results we obtained for the even more translucent alabaster horse head in Fig. 7. Due to its dependence on surface normal PDI cannot reconstruct as much of the surface as our MPS method but the reconstructed surface is slightly smoother, indicating that in this case the MPS could not filter out subsurface structures completely.

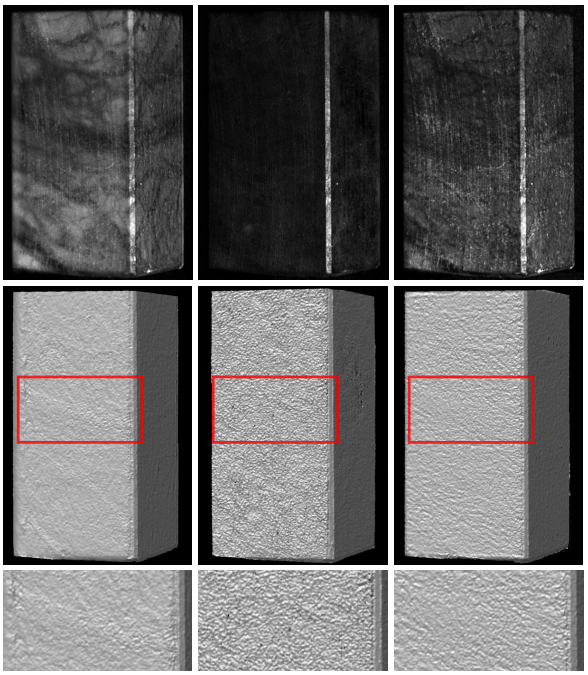

(a) (b) (c)

Figure 6. Direct components and reconstructed 3D shapes for the edge of the alabaster block. (a) PS with $f_x = \frac{1}{8}$ is not sufficient to remove all subsurface scattering. (b) For PDI, $f_x = \frac{1}{8}$, the strength of the recovered direct component is largely dependent on the surface normal resulting in a noisy reconstruction. (c) MPS with $f_x = \frac{1}{8}$ and $f_y = \frac{1}{6}$ yields good results independent of the surface orientation.

5.4. Interreflection Scene

The performance of the three approaches on a different global illumination effect is demonstrated in Fig. 8. The illumination in this scene contains reflections of a glossy sphere as well as interreflections between the two pages of a book, mostly noticeable near the edge. These interreflections heavily corrupt the 3D geometry estimated by standard phase-shifting. The reconstruction based on PDI is so noisy that it is hard to determine how much of the interreflections actually have been filtered out. Applying modulated phase-shifting removes most of the interreflections and produces the most accurate 3D shape. For comparison, the 3D profiles of the edge are shown in Fig. 9. Both the PS and the PDI methods suffer from the strong interreflection, while the MPS method reconstructs the corner geometry very well.

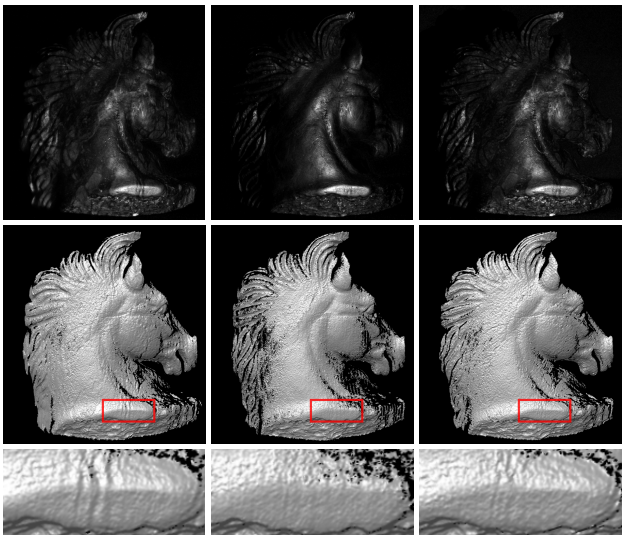

(a) (b) (c)

Figure 7. Direct components and reconstructed 3D shapes for the alabaster horse head. (a) PS with $f_x = \frac{1}{8}$. (b) PDI with $f_x = \frac{1}{8}$. (c) MPS with $f_x = \frac{1}{8}$ and $f_y = \frac{1}{6}$. PDI reconstructs fewer surface points but produces a smoother surface for some parts. The applied frequency for MPS is not sufficient for a perfect separation in this case.

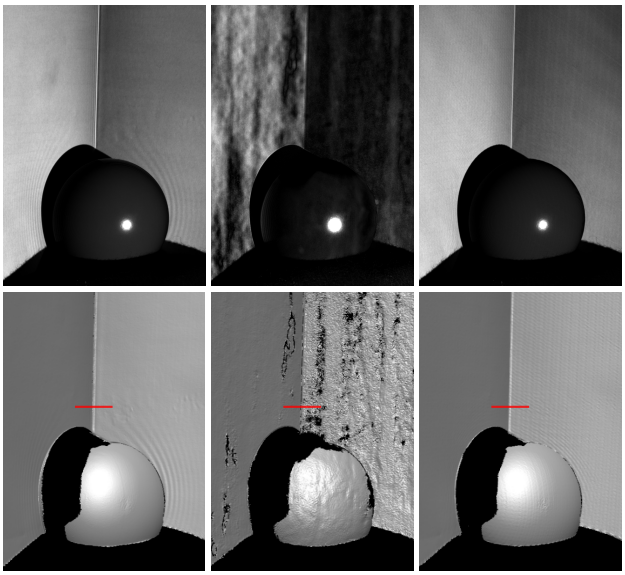

(a) (b) (c)

Figure 8. Strong interreflections by a glossy sphere and between the two pages of a book. We apply the same frequencies as before. (a) PS produces ripples in the final geometry due to the reflections of the sphere. (b) The result by PDI is very noise due to the modified polarization after interreflections. (c) The most accurate reconstruction is achieved using MPS. See Fig. 9 for the profiles along the red lines.

5.5. Two-Pass vs. Single-Pass 2D Separation

For the edge of the alabaster block, Fig. 1 shows the difference between two-pass separation (Sec. 4) we used in all the presented experiments and the minimum-maximum algorithm on 2D patterns [10]. In the 2D minimum-maximum approach, the direct component is estimated from the minimum and maximum intensity values for all measurements of each pixel, while in the two-pass method the separation is performed sequentially along the y and x directions. Although exactly the same input images are used, our two-pass method by exploiting the non-linearity in the analysis results in a much clearer separation where the direct component contains far less of the global subsurface scattering component.

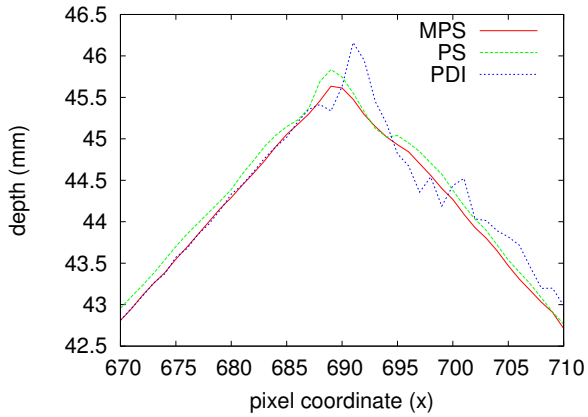

Figure 9. Corner profiles of the scene in Fig. 8. Both PS and PDI show significant artifacts due to the interreflections.

5.6. Limitations

As demonstrated in Fig. 4 and 5 the separation performance of the structured patterns depends on the highest frequency employed. While modulated phase-shifting introduces a principled way of increasing the separation performance for a low-frequency input signal, the carrier frequency is still limited by the projection system. The maximum reliable frequency we could project is $\frac{1}{6}$ since our projector cannot project very high-frequency patterns accurately. The projector introduces serious artifacts (interference-like wave artifacts) when projecting checkerboard with checker size smaller than 3. In Fig. 7(c) a higher frequency would have been needed to completely remove all subsurface scattering. Even at size 3, the projected patterns contains noticeable artifacts, which cause high frequency noise in the result scans. Most of the presented results to a small extent suffer from this problem. It is mostly noticeable in Fig. 8(c), where the smooth paper surface is polluted by small scale noise. This limitation renders modulated phase-shifting inferior to traditional phase-shifting when scanning opaque objects without global illumination effects.

6. Conclusion

Traditional phase-shifting for profilometry usually employs sinusoid patterns where the signal varies only in one direction. Phase-shifting is one of the most robust 3D scanning techniques but the results might still be corrupted by global illumination effects such as subsurface scattering or interreflections. We introduced the concept of modulated phase-shifting where the original one-dimensional pattern is multiplied by a second shifted high-frequency pattern in the other direction. This modulation requires capturing more images but results in significantly improved robustness against pollution due to these global illumination effects.

Compared to 3D scanning techniques based on polarization difference imaging (PDI) [3] our proposed modulation technique is less demanding with regard to the acquisition setup. Our method clearly outperforms PDI for objects with strongly varying surface normals as well as for scenes with strong interreflections.

Moreover, we extended the modulation scheme to general low-frequency functions, *e.g.* an ordinary photograph. This provides a new possibility to enhance the robustness of applications where the frequency of the original signal is rather limited.

An interesting direction for future investigation is a systematic evaluation of different modulation functions and modulation schemes. Another valuable extension is to exploit the general modulation for novel applications.

Acknowledgements

We would like to thank the anonymous reviewers for their valuable comments. Thanks to Martin Fuchs and Andrei Linţu for their proofreading. Thanks to Kuangyu Shi, Naveed Ahmed, and Gernot Ziegler for their objects. We are grateful to Yan Wang for her assistance in the project. This work has been partially funded by the DFG Emmy Noether fellowship (Le 1341/1-1) and the Max Planck Center for Visual Computing and Communication (BMBF-FKZ01IMC01).

References

[1] M. Born, E. Wolf, and A. B. Bhatia. *Principles of Optics*. Cambridge University Press, 1999.

[2] T. Chen, M. Goesele, and H.-P. Seidel. Mesostructure from specularity. In *Proceedings of CVPR*, pages 1825–1832, 2006.

[3] T. Chen, H. Lensch, C. Fuchs, and H.-P. Seidel. Polarization and phase-shifting for 3D scanning of translucent objects. In *Proceedings of CVPR*, 2007.

[4] P. E. Debevec and J. Malik. Recovering high dynamic range radiance maps from photographs. In *SIGGRAPH*, pages 369–378, 1997.

[5] D. C. Ghiglia and M. D. Pritt. *Two-dimensional phase unwrapping: theory, algorithms, and software*. Wiley, New York, 1998.

[6] G. Godin, J.-A. Beraldin, M. Rioux, M. Levoy, L. Cournoyer, and F. Blais. An assessment of laser range measurement of marble surfaces. In *Proceedings of Fifth Conference on optical 3-D measurement techniques*, pages 49–56, 2001.

[7] J. M. Huntley and H. O. Saldner. Temporal phase unwrapping algorithm for automated interferogram analysis. *Appl. Opt.*, 32:3047–3052, 1993.

[8] W.-C. Ma, T. Hawkins, P. Peers, C.-F. Chabert, M. Weiss, and P. Debevec. Rapid acquisition of specular and diffuse normal maps from polarized spherical gradient illumination. In *Proceedings of EGSR*, 2007.

[9] N. J. W. Morris and K. N. Kutulakos. Reconstructing the surface of inhomogeneous transparent scenes by scatter trace photography. In *Proceedings of ICCV*, 2007.

[10] S. K. Nayar, G. Krishnan, M. D. Grossberg, and R. Raskar. Fast separation of direct and global components of a scene using high frequency illumination. *ACM Transactions on Graphics*, 25(3):935–944, 2006.

[11] J. Salvi, J. Pages, and J. Batlle. Pattern codification strategies in structured light systems. *Pattern Recognition*, 37(4):827–849, 2004.

[12] S. M. Seitz, Y. Matsushita, and K. N. Kutulakos. A theory of inverse light transport. In *ICCV*, pages 1440–1447, 2005.

[13] V. Srinivasan, H.-C. Liu, and M. Halioua. Automated phase-measuring profilometry: A phase mapping approach. *Appl. Opt.*, 24:185–188, 1985.

[14] E.-V. Talvala, A. Adams, M. Horowitz, and M. Levoy. Veiling glare in high dynamic range imaging. In *SIGGRAPH '07*, page 37, 2007.

[15] A. Veeraraghavan, R. Raskar, A. Agrawal, A. Mohan, and J. Tumblin. Dappled photography: mask enhanced cameras for heterodyned light fields and coded aperture refocusing. In *SIGGRAPH*, page 69, 2007.

[16] T. Weise, B. Leibe, and L. V. Gool. Fast 3d scanning with automatic motion compensation. In *CVPR*, 2007.

[17] C. Wust and D. W. Capson. Surface profile measurement using color fringe projection. *Mach. Vision Appl.*, 4(3):193–203, 1991.

[18] S. Zhang, X. Li, and S.-T. Yau. Multi-level quality-guided phase unwrapping algorithm for real-time 3-D shape reconstruction. Appl. Opt. 2006.

[19] S. Zhang and S.-T. Yau. Generic nonsinusoidal phase error correction for 3-D shape measurement using a digital video projector. Appl. Opt. 2006.

[20] S. Zhang and S.-T. Yau. High-resolution, real-time absolute 3-D coordinate measurement based on the phase shifting method. *Opt. Express*, 14:2644–2649, 2006.

[21] Z. Zhang. A flexible new technique for camera calibration. *PAMI*, 22(11):1330–1334, 2000.